

Measurement of the spin of the $\Xi(1530)$ resonance

B. Aubert,¹ M. Bona,¹ Y. Karyotakis,¹ J. P. Lees,¹ V. Poireau,¹ X. Prudent,¹ V. Tisserand,¹ A. Zghiche,¹ J. Garra Tico,² E. Grauges,² L. Lopez,³ A. Palano,³ M. Pappagallo,³ G. Eigen,⁴ B. Stugu,⁴ L. Sun,⁴ G. S. Abrams,⁵ M. Battaglia,⁵ D. N. Brown,⁵ J. Button-Shafer,⁵ R. N. Cahn,⁵ R. G. Jacobsen,⁵ J. A. Kadyk,⁵ L. T. Kerth,⁵ Yu. G. Kolomensky,⁵ G. Kukartsev,⁵ G. Lynch,⁵ I. L. Osipenkov,⁵ M. T. Ronan,^{5,*} K. Tackmann,⁵ T. Tanabe,⁵ W. A. Wenzel,⁵ C. M. Hawkes,⁶ N. Soni,⁶ A. T. Watson,⁶ H. Koch,⁷ T. Schroeder,⁷ D. Walker,⁸ D. J. Asgeirsson,⁹ T. Cuhadar-Donszelmann,⁹ B. G. Fulsom,⁹ C. Hearty,⁹ T. S. Mattison,⁹ J. A. McKenna,⁹ M. Barrett,¹⁰ A. Khan,¹⁰ M. Saleem,¹⁰ L. Teodorescu,¹⁰ V. E. Blinov,¹¹ A. D. Bukin,¹¹ A. R. Buzykaev,¹¹ V. P. Druzhinin,¹¹ V. B. Golubev,¹¹ A. P. Onuchin,¹¹ S. I. Serednyakov,¹¹ Yu. I. Skovpen,¹¹ E. P. Solodov,¹¹ K. Yu. Todyshev,¹¹ M. Bondioli,¹² S. Curry,¹² I. Eschrich,¹² D. Kirkby,¹² A. J. Lankford,¹² P. Lund,¹² M. Mandelkern,¹² E. C. Martin,¹² D. P. Stoker,¹² S. Abachi,¹³ C. Buchanan,¹³ J. W. Gary,¹⁴ F. Liu,¹⁴ O. Long,¹⁴ B. C. Shen,^{14,*} G. M. Vitug,¹⁴ Z. Yasin,¹⁴ L. Zhang,¹⁴ H. P. Paar,¹⁵ S. Rahatlou,¹⁵ V. Sharma,¹⁵ C. Campagnari,¹⁶ T. M. Hong,¹⁶ D. Kovalskyi,¹⁶ M. A. Mazur,¹⁶ J. D. Richman,¹⁶ T. W. Beck,¹⁷ A. M. Eisner,¹⁷ C. J. Flacco,¹⁷ C. A. Heusch,¹⁷ J. Kroseberg,¹⁷ W. S. Lockman,¹⁷ T. Schalk,¹⁷ B. A. Schumm,¹⁷ A. Seiden,¹⁷ M. G. Wilson,¹⁷ L. O. Winstrom,¹⁷ E. Chen,¹⁸ C. H. Cheng,¹⁸ D. A. Doll,¹⁸ B. Echenard,¹⁸ F. Fang,¹⁸ D. G. Hitlin,¹⁸ I. Narsky,¹⁸ T. Piatenko,¹⁸ F. C. Porter,¹⁸ R. Andreassen,¹⁹ G. Mancinelli,¹⁹ B. T. Meadows,¹⁹ K. Mishra,¹⁹ M. D. Sokoloff,¹⁹ F. Blanc,²⁰ P. C. Bloom,²⁰ W. T. Ford,²⁰ J. F. Hirschauer,²⁰ A. Kreisel,²⁰ M. Nagel,²⁰ U. Nauenberg,²⁰ A. Olivas,²⁰ J. G. Smith,²⁰ K. A. Ulmer,²⁰ S. R. Wagner,²⁰ R. Ayad,^{21,+} A. M. Gabareen,²¹ A. Soffer,^{21,‡} W. H. Toki,²¹ R. J. Wilson,²¹ D. D. Altenburg,²² E. Feltresi,²² A. Hauke,²² H. Jasper,²² M. Karbach,²² J. Merkel,²² A. Petzold,²² B. Spaan,²² K. Wacker,²² V. Klose,²³ M. J. Kobel,²³ H. M. Lacker,²³ W. F. Mader,²³ R. Nogowski,²³ J. Schubert,²³ K. R. Schubert,²³ R. Schwierz,²³ J. E. Sundermann,²³ A. Volk,²³ D. Bernard,²⁴ G. R. Bonneaud,²⁴ E. Latour,²⁴ Ch. Thiebaux,²⁴ M. Verderi,²⁴ P. J. Clark,²⁵ W. Gradl,²⁵ S. Playfer,²⁵ A. I. Robertson,²⁵ J. E. Watson,²⁵ M. Andreotti,²⁶ D. Bettoni,²⁶ C. Bozzi,²⁶ R. Calabrese,²⁶ A. Cecchi,²⁶ G. Cibinetto,²⁶ P. Franchini,²⁶ E. Luppi,²⁶ M. Negrini,²⁶ A. Petrella,²⁶ L. Piemontese,²⁶ E. Prencipe,²⁶ V. Santoro,²⁶ F. Anulli,²⁷ R. Baldini-Feroli,²⁷ A. Calcaterra,²⁷ R. de Sangro,²⁷ G. Finocchiaro,²⁷ S. Pacetti,²⁷ P. Patteri,²⁷ I. M. Peruzzi,^{27,§} M. Piccolo,²⁷ M. Rama,²⁷ A. Zallo,²⁷ A. Buzzo,²⁸ R. Contri,²⁸ M. Lo Vetere,²⁸ M. M. Macri,²⁸ M. R. Monge,²⁸ S. Passaggio,²⁸ C. Patrignani,²⁸ E. Robutti,²⁸ A. Santroni,²⁸ S. Tosi,²⁸ K. S. Chaisanguanthum,²⁹ M. Morii,²⁹ R. S. Dubitzky,³⁰ J. Marks,³⁰ S. Schenk,³⁰ U. Uwer,³⁰ D. J. Bard,³¹ P. D. Dauncey,³¹ J. A. Nash,³¹ W. Panduro Vazquez,³¹ M. Tibbetts,³¹ P. K. Behera,³² X. Chai,³² M. J. Charles,³² U. Mallik,³² J. Cochran,³³ H. B. Crawley,³³ L. Dong,³³ V. Eyges,³³ W. T. Meyer,³³ S. Prell,³³ E. I. Rosenberg,³³ A. E. Rubin,³³ Y. Y. Gao,³⁴ A. V. Gritsan,³⁴ Z. J. Guo,³⁴ C. K. Lae,³⁴ A. G. Denig,³⁵ M. Fritsch,³⁵ G. Schott,³⁵ N. Arnaud,³⁶ J. Béquilleux,³⁶ A. D'Orazio,³⁶ M. Davier,³⁶ J. Firmino da Costa,³⁶ G. Grosdidier,³⁶ A. Höcker,³⁶ V. Lepeltier,³⁶ F. Le Diberder,³⁶ A. M. Lutz,³⁶ S. Pruvot,³⁶ P. Roudeau,³⁶ M. H. Schune,³⁶ J. Serrano,³⁶ V. Sordini,³⁶ A. Stocchi,³⁶ W. F. Wang,³⁶ G. Wormser,³⁶ D. J. Lange,³⁷ D. M. Wright,³⁷ I. Bingham,³⁸ J. P. Burke,³⁸ C. A. Chavez,³⁸ J. R. Fry,³⁸ E. Gabathuler,³⁸ R. Gamet,³⁸ D. E. Hutchcroft,³⁸ D. J. Payne,³⁸ C. Touramanis,³⁸ A. J. Bevan,³⁹ K. A. George,³⁹ F. Di Lodovico,³⁹ R. Sacco,³⁹ M. Sigamani,³⁹ G. Cowan,⁴⁰ H. U. Flaecher,⁴⁰ D. A. Hopkins,⁴⁰ S. Paramesvaran,⁴⁰ F. Salvatore,⁴⁰ A. C. Wren,⁴⁰ D. N. Brown,⁴¹ C. L. Davis,⁴¹ K. E. Alwyn,⁴² N. R. Barlow,⁴² R. J. Barlow,⁴² Y. M. Chia,⁴² C. L. Edgar,⁴² G. D. Lafferty,⁴² T. J. West,⁴² J. I. Yi,⁴² J. Anderson,⁴³ C. Chen,⁴³ A. Jawahery,⁴³ D. A. Roberts,⁴³ G. Simi,⁴³ J. M. Tuggle,⁴³ C. Dallapiccola,⁴⁴ S. S. Hertzbach,⁴⁴ X. Li,⁴⁴ E. Salvati,⁴⁴ S. Saremi,⁴⁴ R. Cowan,⁴⁵ D. Dujmic,⁴⁵ P. H. Fisher,⁴⁵ K. Koeneke,⁴⁵ G. Sciolla,⁴⁵ M. Spitznagel,⁴⁵ F. Taylor,⁴⁵ R. K. Yamamoto,⁴⁵ M. Zhao,⁴⁵ S. E. Mclachlin,^{46,*} P. M. Patel,⁴⁶ S. H. Robertson,⁴⁶ A. Lazzaro,⁴⁷ V. Lombardo,⁴⁷ F. Palombo,⁴⁷ J. M. Bauer,⁴⁸ L. Cremaldi,⁴⁸ V. Eschenburg,⁴⁸ R. Godang,⁴⁸ R. Kroeger,⁴⁸ D. A. Sanders,⁴⁸ D. J. Summers,⁴⁸ H. W. Zhao,⁴⁸ S. Brunet,⁴⁹ D. Côté,⁴⁹ M. Simard,⁴⁹ P. Taras,⁴⁹ F. B. Viaud,⁴⁹ H. Nicholson,⁵⁰ G. De Nardo,⁵¹ L. Lista,⁵¹ D. Monorchio,⁵¹ C. Sciacca,⁵¹ M. A. Baak,⁵² G. Raven,⁵² H. L. Snoek,⁵² C. P. Jessop,⁵³ K. J. Knoepfel,⁵³ J. M. LoSecco,⁵³ G. Benelli,⁵⁴ L. A. Corwin,⁵⁴ K. Honscheid,⁵⁴ H. Kagan,⁵⁴ R. Kass,⁵⁴ J. P. Morris,⁵⁴ A. M. Rahimi,⁵⁴ J. J. Regensburger,⁵⁴ S. J. Sekula,⁵⁴ Q. K. Wong,⁵⁴ N. L. Blount,⁵⁵ J. Brau,⁵⁵ R. Frey,⁵⁵ O. Igonkina,⁵⁵ J. A. Kolb,⁵⁵ M. Lu,⁵⁵ R. Rahmat,⁵⁵ N. B. Sinev,⁵⁵ D. Strom,⁵⁵ J. Strube,⁵⁵ E. Torrence,⁵⁵ G. Castelli,⁵⁶ N. Gagliardi,⁵⁶ A. Gaz,⁵⁶ M. Margoni,⁵⁶ M. Morandin,⁵⁶ M. Posocco,⁵⁶ M. Rotondo,⁵⁶ F. Simonetto,⁵⁶ R. Stroili,⁵⁶ C. Voci,⁵⁶ P. del Amo Sanchez,⁵⁷ E. Ben-Haim,⁵⁷ H. Briand,⁵⁷ G. Calderini,⁵⁷ J. Chauveau,⁵⁷ P. David,⁵⁷ L. Del Buono,⁵⁷ O. Hamon,⁵⁷ Ph. Leruste,⁵⁷ J. Malclès,⁵⁷ J. Ocariz,⁵⁷ A. Perez,⁵⁷ J. Prendki,⁵⁷ L. Gladney,⁵⁸ M. Biasini,⁵⁹ R. Covarelli,⁵⁹ E. Manoni,⁵⁹ C. Angelini,⁶⁰ G. Batignani,⁶⁰ S. Bettarini,⁶⁰ M. Carpinelli,^{60,||} A. Cervelli,⁶⁰ F. Forti,⁶⁰ M. A. Giorgi,⁶⁰ A. Lusiani,⁶⁰ G. Marchiori,⁶⁰ M. Morganti,⁶⁰ N. Neri,⁶⁰ E. Paoloni,⁶⁰ G. Rizzo,⁶⁰ J. J. Walsh,⁶⁰ J. Biesiada,⁶¹ Y. P. Lau,⁶¹

D. Lopes Pegna,⁶¹ C. Lu,⁶¹ J. Olsen,⁶¹ A. J. S. Smith,⁶¹ A. V. Telnov,⁶¹ E. Baracchini,⁶² G. Cavoto,⁶² D. del Re,⁶² E. Di Marco,⁶² R. Faccini,⁶² F. Ferrarotto,⁶² F. Ferroni,⁶² M. Gaspero,⁶² P. D. Jackson,⁶² M. A. Mazzoni,⁶² S. Morganti,⁶² G. Piredda,⁶² F. Polci,⁶² F. Renga,⁶² C. Voena,⁶² M. Ebert,⁶³ T. Hartmann,⁶³ H. Schröder,⁶³ R. Waldi,⁶³ T. Adye,⁶⁴ B. Franek,⁶⁴ E. O. Olaiya,⁶⁴ W. Roethel,⁶⁴ F. F. Wilson,⁶⁴ S. Emery,⁶⁵ M. Escalier,⁶⁵ A. Gaidot,⁶⁵ S. F. Ganzhur,⁶⁵ G. Hamel de Monchenault,⁶⁵ W. Kozanecki,⁶⁵ G. Vasseur,⁶⁵ Ch. Yèche,⁶⁵ M. Zito,⁶⁵ X. R. Chen,⁶⁶ H. Liu,⁶⁶ W. Park,⁶⁶ M. V. Purohit,⁶⁶ R. M. White,⁶⁶ J. R. Wilson,⁶⁶ M. T. Allen,⁶⁷ D. Aston,⁶⁷ R. Bartoldus,⁶⁷ P. Bechtle,⁶⁷ J. F. Benitez,⁶⁷ R. Cenci,⁶⁷ J. P. Coleman,⁶⁷ M. R. Convery,⁶⁷ J. C. Dingfelder,⁶⁷ J. Dorfan,⁶⁷ G. P. Dubois-Felsmann,⁶⁷ W. Dunwoodie,⁶⁷ R. C. Field,⁶⁷ T. Glanzman,⁶⁷ S. J. Gowdy,⁶⁷ M. T. Graham,⁶⁷ P. Grenier,⁶⁷ C. Hast,⁶⁷ W. R. Innes,⁶⁷ J. Kaminski,⁶⁷ M. H. Kelsey,⁶⁷ H. Kim,⁶⁷ P. Kim,⁶⁷ M. L. Kocian,⁶⁷ D. W. G. S. Leith,⁶⁷ S. Li,⁶⁷ B. Lindquist,⁶⁷ S. Luitz,⁶⁷ V. Luth,⁶⁷ H. L. Lynch,⁶⁷ D. B. MacFarlane,⁶⁷ H. Marsiske,⁶⁷ R. Messner,⁶⁷ D. R. Muller,⁶⁷ H. Neal,⁶⁷ S. Nelson,⁶⁷ C. P. O'Grady,⁶⁷ I. Ofte,⁶⁷ A. Perazzo,⁶⁷ M. Perl,⁶⁷ B. N. Ratcliff,⁶⁷ A. Roodman,⁶⁷ A. A. Salnikov,⁶⁷ R. H. Schindler,⁶⁷ J. Schwiening,⁶⁷ A. Snyder,⁶⁷ D. Su,⁶⁷ M. K. Sullivan,⁶⁷ K. Suzuki,⁶⁷ S. K. Swain,⁶⁷ J. M. Thompson,⁶⁷ J. Va'vra,⁶⁷ A. P. Wagner,⁶⁷ M. Weaver,⁶⁷ W. J. Wisniewski,⁶⁷ M. Wittgen,⁶⁷ D. H. Wright,⁶⁷ H. W. Wulsin,⁶⁷ A. K. Yarritu,⁶⁷ K. Yi,⁶⁷ C. C. Young,⁶⁷ V. Ziegler,⁶⁷ P. R. Burchat,⁶⁸ A. J. Edwards,⁶⁸ S. A. Majewski,⁶⁸ T. S. Miyashita,⁶⁸ B. A. Petersen,⁶⁸ L. Wilden,⁶⁸ S. Ahmed,⁶⁹ M. S. Alam,⁶⁹ R. Bula,⁶⁹ J. A. Ernst,⁶⁹ B. Pan,⁶⁹ M. A. Saeed,⁶⁹ S. B. Zain,⁶⁹ S. M. Spanier,⁷⁰ B. J. Wogslund,⁷⁰ R. Eckmann,⁷¹ J. L. Ritchie,⁷¹ A. M. Ruland,⁷¹ C. J. Schilling,⁷¹ R. F. Schwitters,⁷¹ J. M. Izen,⁷² X. C. Lou,⁷² S. Ye,⁷² F. Bianchi,⁷³ D. Gamba,⁷³ M. Pelliccioni,⁷³ M. Bomben,⁷⁴ L. Bosisio,⁷⁴ C. Cartaro,⁷⁴ F. Cossutti,⁷⁴ G. Della Ricca,⁷⁴ L. Lancieri,⁷⁴ L. Vitale,⁷⁴ V. Azzolini,⁷⁵ N. Lopez-March,⁷⁵ F. Martinez-Vidal,⁷⁵ D. A. Milanes,⁷⁵ A. Oyanguren,⁷⁵ J. Albert,⁷⁶ Sw. Banerjee,⁷⁶ B. Bhuyan,⁷⁶ K. Hamano,⁷⁶ R. Kowalewski,⁷⁶ I. M. Nugent,⁷⁶ J. M. Roney,⁷⁶ R. J. Sobie,⁷⁶ T. J. Gershon,⁷⁷ P. F. Harrison,⁷⁷ J. Ilic,⁷⁷ T. E. Latham,⁷⁷ G. B. Mohanty,⁷⁷ H. R. Band,⁷⁸ X. Chen,⁷⁸ S. Dasu,⁷⁸ K. T. Flood,⁷⁸ P. E. Kutter,⁷⁸ Y. Pan,⁷⁸ M. Pierini,⁷⁸ R. Prepost,⁷⁸ C. O. Vuosalo,⁷⁸ and S. L. Wu⁷⁸

(BABAR Collaboration)

¹Laboratoire de Physique des Particules, IN2P3/CNRS et Université de Savoie, F-74941 Annecy-Le-Vieux, France

²Universitat de Barcelona, Facultat de Física, Departament ECM, E-08028 Barcelona, Spain

³Università di Bari, Dipartimento di Fisica and INFN, I-70126 Bari, Italy

⁴University of Bergen, Institute of Physics, N-5007 Bergen, Norway

⁵Lawrence Berkeley National Laboratory and University of California, Berkeley, California 94720, USA

⁶University of Birmingham, Birmingham, B15 2TT, United Kingdom

⁷Ruhr Universität Bochum, Institut für Experimentalphysik 1, D-44780 Bochum, Germany

⁸University of Bristol, Bristol BS8 1TL, United Kingdom

⁹University of British Columbia, Vancouver, British Columbia, Canada V6T 1Z1

¹⁰Brunel University, Uxbridge, Middlesex UB8 3PH, United Kingdom

¹¹Budker Institute of Nuclear Physics, Novosibirsk 630090, Russia

¹²University of California at Irvine, Irvine, California 92697, USA

¹³University of California at Los Angeles, Los Angeles, California 90024, USA

¹⁴University of California at Riverside, Riverside, California 92521, USA

¹⁵University of California at San Diego, La Jolla, California 92093, USA

¹⁶University of California at Santa Barbara, Santa Barbara, California 93106, USA

¹⁷University of California at Santa Cruz, Institute for Particle Physics, Santa Cruz, California 95064, USA

¹⁸California Institute of Technology, Pasadena, California 91125, USA

¹⁹University of Cincinnati, Cincinnati, Ohio 45221, USA

²⁰University of Colorado, Boulder, Colorado 80309, USA

²¹Colorado State University, Fort Collins, Colorado 80523, USA

²²Universität Dortmund, Institut für Physik, D-44221 Dortmund, Germany

²³Technische Universität Dresden, Institut für Kern- und Teilchenphysik, D-01062 Dresden, Germany

²⁴Laboratoire Leprince-Ringuet, CNRS/IN2P3, Ecole Polytechnique, F-91128 Palaiseau, France

²⁵University of Edinburgh, Edinburgh EH9 3JZ, United Kingdom

²⁶Università di Ferrara, Dipartimento di Fisica and INFN, I-44100 Ferrara, Italy

²⁷Laboratori Nazionali di Frascati dell'INFN, I-00044 Frascati, Italy

²⁸Università di Genova, Dipartimento di Fisica and INFN, I-16146 Genova, Italy

²⁹Harvard University, Cambridge, Massachusetts 02138, USA

³⁰Universität Heidelberg, Physikalisches Institut, Philosophenweg 12, D-69120 Heidelberg, Germany

³¹Imperial College London, London, SW7 2AZ, United Kingdom

³²University of Iowa, Iowa City, Iowa 52242, USA

- ³³Iowa State University, Ames, Iowa 50011-3160, USA
³⁴Johns Hopkins University, Baltimore, Maryland 21218, USA
³⁵Universität Karlsruhe, Institut für Experimentelle Kernphysik, D-76021 Karlsruhe, Germany
³⁶Laboratoire de l'Accélérateur Linéaire, IN2P3/CNRS et Université Paris-Sud 11, Centre Scientifique d'Orsay, B. P. 34, F-91898 ORSAY Cedex, France
³⁷Lawrence Livermore National Laboratory, Livermore, California 94550, USA
³⁸University of Liverpool, Liverpool L69 7ZE, United Kingdom
³⁹Queen Mary, University of London, E1 4NS, United Kingdom
⁴⁰University of London, Royal Holloway and Bedford New College, Egham, Surrey TW20 0EX, United Kingdom
⁴¹University of Louisville, Louisville, Kentucky 40292, USA
⁴²University of Manchester, Manchester M13 9PL, United Kingdom
⁴³University of Maryland, College Park, Maryland 20742, USA
⁴⁴University of Massachusetts, Amherst, Massachusetts 01003, USA
⁴⁵Massachusetts Institute of Technology, Laboratory for Nuclear Science, Cambridge, Massachusetts 02139, USA
⁴⁶McGill University, Montréal, Québec, Canada H3A 2T8
⁴⁷Università di Milano, Dipartimento di Fisica and INFN, I-20133 Milano, Italy
⁴⁸University of Mississippi, University, Mississippi 38677, USA
⁴⁹Université de Montréal, Physique des Particules, Montréal, Québec, Canada H3C 3J7
⁵⁰Mount Holyoke College, South Hadley, Massachusetts 01075, USA
⁵¹Università di Napoli Federico II, Dipartimento di Scienze Fisiche and INFN, I-80126, Napoli, Italy
⁵²NIKHEF, National Institute for Nuclear Physics and High Energy Physics, NL-1009 DB Amsterdam, The Netherlands
⁵³University of Notre Dame, Notre Dame, Indiana 46556, USA
⁵⁴Ohio State University, Columbus, Ohio 43210, USA
⁵⁵University of Oregon, Eugene, Oregon 97403, USA
⁵⁶Università di Padova, Dipartimento di Fisica and INFN, I-35131 Padova, Italy
⁵⁷Laboratoire de Physique Nucléaire et de Hautes Energies, IN2P3/CNRS, Université Pierre et Marie Curie-Paris6, Université Denis Diderot-Paris7, F-75252 Paris, France
⁵⁸University of Pennsylvania, Philadelphia, Pennsylvania 19104, USA
⁵⁹Università di Perugia, Dipartimento di Fisica and INFN, I-06100 Perugia, Italy
⁶⁰Università di Pisa, Dipartimento di Fisica, Scuola Normale Superiore and INFN, I-56127 Pisa, Italy
⁶¹Princeton University, Princeton, New Jersey 08544, USA
⁶²Università di Roma La Sapienza, Dipartimento di Fisica and INFN, I-00185 Roma, Italy
⁶³Universität Rostock, D-18051 Rostock, Germany
⁶⁴Rutherford Appleton Laboratory, Chilton, Didcot, Oxon, OX11 0QX, United Kingdom
⁶⁵DSM/Dapnia, CEA/Saclay, F-91191 Gif-sur-Yvette, France
⁶⁶University of South Carolina, Columbia, South Carolina 29208, USA
⁶⁷Stanford Linear Accelerator Center, Stanford, California 94309, USA
⁶⁸Stanford University, Stanford, California 94305-4060, USA
⁶⁹State University of New York, Albany, New York 12222, USA
⁷⁰University of Tennessee, Knoxville, Tennessee 37996, USA
⁷¹University of Texas at Austin, Austin, Texas 78712, USA
⁷²University of Texas at Dallas, Richardson, Texas 75083, USA
⁷³Università di Torino, Dipartimento di Fisica Sperimentale and INFN, I-10125 Torino, Italy
⁷⁴Università di Trieste, Dipartimento di Fisica and INFN, I-34127 Trieste, Italy
⁷⁵IFIC, Universitat de Valencia-CSIC, E-46071 Valencia, Spain
⁷⁶University of Victoria, Victoria, British Columbia, Canada V8W 3P6
⁷⁷Department of Physics, University of Warwick, Coventry CV4 7AL, United Kingdom
⁷⁸University of Wisconsin, Madison, Wisconsin 53706, USA

(Received 12 March 2008; published 11 August 2008)

The properties of the $\Xi(1530)$ resonance are investigated in the $\Lambda_c^+ \rightarrow \Xi^- \pi^+ K^+$ decay process. The data sample was collected with the BABAR detector at the SLAC PEP-II asymmetric-energy e^+e^- collider operating at center-of-mass energies 10.58 and 10.54 GeV. The corresponding integrated luminosity is approximately 230 fb^{-1} . The spin of the $\Xi(1530)$ is established to be $3/2$. The existence of an S -wave

*Deceased.

[†]Now at Temple University, Philadelphia, PA 19122, USA.

[‡]Now at Tel Aviv University, Tel Aviv, 69978, Israel.

[§]Also with Università di Perugia, Dipartimento di Fisica, Perugia, Italy.

^{||}Also with Università di Sassari, Sassari, Italy.

amplitude in the $\Xi^- \pi^+$ system is inferred, and its interference with the $\Xi(1530)^0$ amplitude provides the first clear demonstration of the Breit-Wigner phase motion expected for the $\Xi(1530)$. The $P_1(\cos\theta_{\Xi^-})$ Legendre polynomial moment indicates the presence of a significant S -wave amplitude for $\Xi^- \pi^+$ mass values above 1.6 GeV/ c^2 , and a dip in the mass distribution at approximately 1.7 GeV/ c^2 is interpreted as due to the coherent addition of a $\Xi(1690)^0$ contribution to this amplitude. This would imply $J^P = 1/2^-$ for the $\Xi(1690)$. Attempts at fitting the $\Xi(1530)^0$ line shape yield unsatisfactory results, and this failure is attributed to interference effects associated with the amplitudes describing the $K^+ \pi^+$ and/or $\Xi^- K^+$ systems.

DOI: [10.1103/PhysRevD.78.034008](https://doi.org/10.1103/PhysRevD.78.034008)

PACS numbers: 13.30.Eg, 14.20.Jn, 14.20.Lq

I. INTRODUCTION

The $\Xi(1530)$ is the only cascade resonance whose properties are reasonably well understood. It decays $\sim 100\%$ to $\Xi\pi$ and $<4\%$ to $\Xi\gamma$ [1], and its mass [PDG fit: $m(\Xi(1530)^0) = 1531.80 \pm 0.32$ MeV/ c^2] and width [PDG fit: $\Gamma(\Xi(1530)^0) = 0.1 \pm 0.5$ MeV] are reasonably well known [1]. A spin-parity analysis of data on the reactions $K^- p \rightarrow \Xi(1530)^0 K^+$ carried out by Schlein *et al.* [2] showed that $J^P = 3/2^+$ (i.e., the P wave) or $J^P = 5/2^-$ (i.e., the D wave) is favored, and that the data are consistent with $J \geq 3/2$; however, they stated that spin $>3/2$ is not required and, on this basis, concluded that $J^P = 3/2^+$. This conclusion was supported by Button-Schafer *et al.* [3] in a similar analysis. Both experiments ruled out $J = 1/2$, but the claim that $J > 3/2$ was not required was the basis for the conclusion that $J^P = 3/2^+$. In the present paper, the Ω^- spin analysis procedures described in Ref. [4] are extended to the quasi-two-body decay $\Lambda_c^+ \rightarrow (\Xi^- \pi^+) K^+$, for which the $\Xi^- \pi^+$ invariant mass distribution exhibits a dominant $\Xi(1530)^0$ signal [5]. Under the assumption that the Λ_c^+ has spin $1/2$, it is established that the $\Xi(1530)$ has spin $3/2$. On the basis of the analyses of Refs. [2,3], it follows that positive parity is established.

The data sample and event selection procedures are described in Sec. II, and the $\Xi(1530)$ spin measurement is presented in Sec. III. In Sec. IV, the amplitude structure in the $\Xi(1530)$ region is investigated in some detail, and this is followed by an examination of the $\Xi^- \pi^+$ system at higher mass values in Sec. V. The unsuccessful attempts at precise measurements of the mass and width of the $\Xi(1530)^0$ are presented in Sec. VI, and their implications considered. Finally, the conclusions drawn from this analysis are summarized in Sec. VII.

II. THE BABAR DETECTOR AND $\Lambda_c^+ \rightarrow \Xi^- \pi^+ K^+$ EVENT SELECTION

The data sample used for this analysis was collected with the *BABAR* detector at the PEP-II asymmetric-energy e^+e^- collider operating at center-of-mass (c.m.) energies 10.58 and 10.54 GeV, and corresponds to a total integrated luminosity of about 230 fb $^{-1}$.

Charged particles are detected with a five-layer, double-sided silicon vertex tracker (SVT) and a 40-layer drift

chamber (DCH) with a helium-isobutane gas mixture, placed in a 1.5-T solenoidal field produced by a superconducting magnet. The charged-particle momentum resolution is approximately $(\delta p_T/p_T)^2 = (0.0013 p_T)^2 + (0.0045)^2$, where p_T is the transverse momentum in GeV/ c . The SVT, with a typical single-hit resolution of 10 μm , measures the impact parameters of charged-particle tracks in both the plane transverse to the beam direction and along the collision axis.

Charged-particle types are identified from the ionization energy loss (dE/dx) measured in the DCH and SVT, and from the Cherenkov radiation detected in a ring-imaging Cherenkov device. Photons are detected by a CsI(Tl) electromagnetic calorimeter with an energy resolution $\sigma(E)/E = 0.023 \cdot (E/\text{GeV})^{-1/4} \oplus 0.019$.

The return yoke of the superconducting coil is instrumented with resistive plate chambers for the identification of muons and the detection of neutral hadrons. The detector is described in detail in Ref. [6].

The selection of Λ_c^+ candidates requires the intermediate reconstruction of events consistent with $\Xi^- \rightarrow \Lambda \pi^-$ and $\Lambda \rightarrow p \pi^-$. Particle identification (PID) selectors based on specific energy loss (dE/dx) and Cherenkov angle measurements are used to identify the proton, pion, and kaon final state tracks [6]. Each intermediate state candidate is required to have invariant mass within a $\pm 3\sigma$ window centered on the fitted peak position of the relevant distribution, where σ is the mass resolution obtained from the fit. A fit is then performed to the complete decay topology with the Λ and Ξ^- candidates constrained to their known mass values [1]. The fit probability is required to be greater than 0.001 in order to ensure simultaneous satisfaction of the topological and mass constraint requirements; this reduces combinatorial background significantly and retains good signal efficiency. Since each weakly decaying intermediate state (i.e., hyperon) is long-lived, an improvement of the signal-to-background ratio is achieved by requiring that the decay vertex of each hyperon be displaced from its point of origin in the direction of its momentum vector. The distance between the $\Xi^- K^+ \pi^+$ vertex and the Ξ^- decay vertex in the plane perpendicular to the collision axis must exceed 1.5 mm in the Ξ^- direction, and the distance between the Ξ^- and Λ decay vertices must exceed 1.5 mm in the direction of the Λ momentum vector. Finally, the momentum of the Λ_c^+

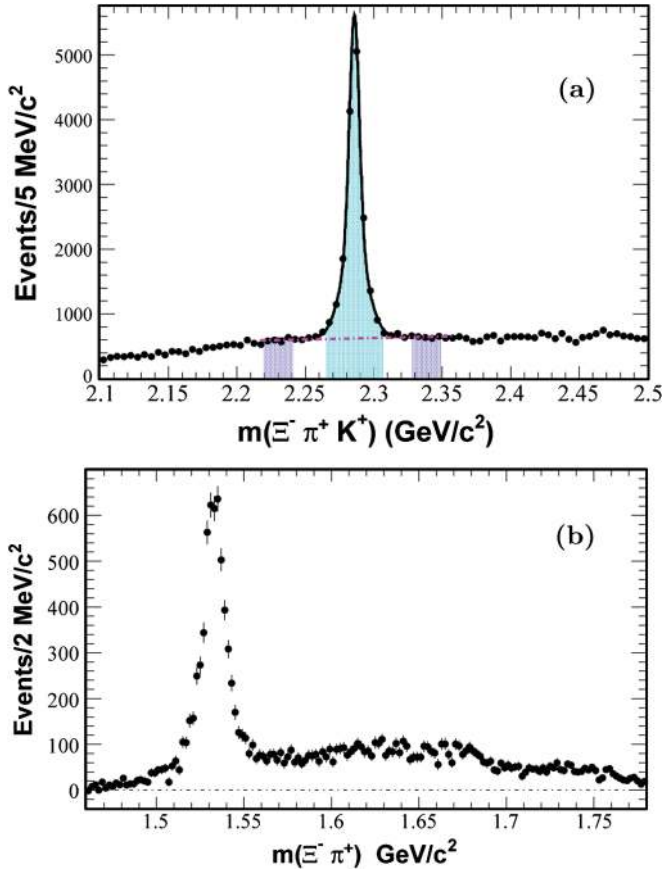


FIG. 1 (color). (a) The uncorrected $\Xi^- \pi^+ K^+$ invariant mass spectrum. The curve results from the fit described in the text. The dot-dashed line indicates the fitted background contribution. The shaded areas delimit the signal (light area) and mass-sideband (dark area) regions. (b) The uncorrected Λ_c^+ -mass-sideband-subtracted $\Xi^- \pi^+$ invariant mass projection for $\Xi^- \pi^+ K^+$ candidates. In each figure, the points with error bars represent the data.

candidate in the e^+e^- c.m. frame p^* is required to be greater than 2.0 GeV/c , since it is found empirically that this significantly reduces combinatorial background. The invariant mass spectrum of Λ_c^+ candidates which satisfy these selection criteria before efficiency correction is shown in Fig. 1(a). A signal yield of $13\,035 \pm 163$ events is obtained from a fit which makes use of a signal function consisting of two Gaussians with a common center and a linear background function to the mass region 2.225–2.360 GeV/c^2 . The fit yields half-width–half-maximum 5.1 MeV/c^2 and has chi-squared per degree of freedom (χ^2/NDF) 19.6/20.

III. $\Xi(1530)$ SPIN MEASUREMENT

The Dalitz plot for $\Lambda_c^+ \rightarrow \Xi^- \pi^+ K^+$ (Fig. 2) is dominated by the contribution from $\Lambda_c^+ \rightarrow \Xi(1530)^0 K^+$, where $\Xi(1530)^0 \rightarrow \Xi^- \pi^+$ is a strong decay. There is evidence for only one resonant structure, seen as the clear band at the nominal mass squared of the $\Xi(1530)^0$. The background

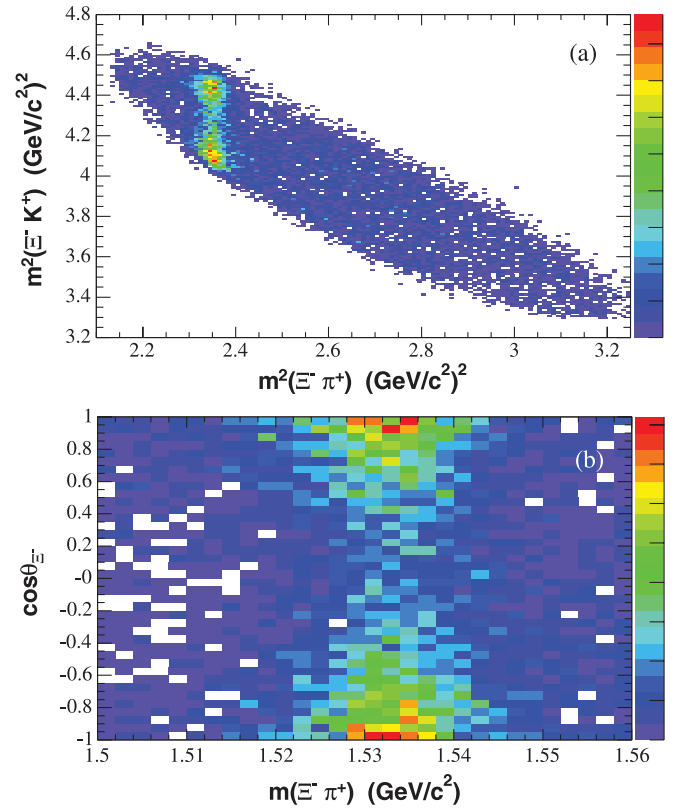


FIG. 2 (color). (a) The Dalitz plot of $\Xi^- K^+$ versus $\Xi^- \pi^+$ invariant mass squared for the Λ_c^+ signal region. (b) The corresponding rectangular Dalitz plot for the $\Xi(1530)^0$ mass region.

events in the signal region of Fig. 1(a) are represented by the events from the combined sideband regions indicated in this figure, which correspond to the same mass range [7]. A corrected distribution associated with the Λ_c^+ signal is obtained by subtraction (bin by bin) of the corresponding distribution for the sidebands from that for the signal region. This procedure is described as “sideband subtraction,” and assumes linear mass dependence of the background. The sideband-subtracted projection of the $\Xi^- \pi^+$ invariant mass for the Λ_c^+ signal region of Fig. 1(a) is shown in Fig. 1(b).

The helicity formalism [8,9] is applied to the quasi-two-body decay $\Lambda_c^+ \rightarrow K^+ \Xi(1530)^0$ in order to examine the implications of various $\Xi(1530)^0$ spin hypotheses for the angular distribution of the Ξ^- from $\Xi(1530)^0$ decay, under the assumption that the $\Xi(1530)^0$ mass region is dominated by a single spin state. As in Ref. [4], it is assumed that the spin of the charm baryon is 1/2. The choice of spin quantization axis along the direction of the $\Xi(1530)^0$ in the charm baryon rest-frame (r.f.) has the result that the $\Xi(1530)^0$ inherits the spin projection of the charm baryon, since any orbital angular momentum in the charm baryon decay has no projection in this direction. It follows that, regardless of the spin J of the $\Xi(1530)^0$, the density matrix which describes the $\Xi(1530)^0$ sample is diagonal, with nonzero values only for the $\pm 1/2$ spin projection elements;

i.e., the helicity λ_i of the $\Xi(1530)^0$ can take only the values $\pm 1/2$. Since the final states Ξ^- and π^+ have spin values $1/2$ and 0 , respectively, the net final state helicity λ_f can also take only the values $\pm 1/2$. The helicity angle θ_{Ξ^-} is defined as the angle between the direction of the Ξ^- in the r.f. of the $\Xi(1530)^0$ and the quantization axis. Following the formalism of Ref. [4], the angular distribution of the Ξ^- is then given by the total intensity,

$$I \propto \sum_{\lambda_i, \lambda_f} \rho_{ii} |A_{\lambda_f}^J D_{\lambda_i \lambda_f}^{J*}(\phi, \theta_{\Xi^-}, 0)|^2, \quad (1)$$

where the ρ_{ii} ($i = \pm 1/2$) are the diagonal density matrix elements inherited from the charm baryon, and the sum is over all initial and final helicity states. The transition matrix element $A_{\lambda_f}^J$ represents the coupling of the $\Xi(1530)^0$ to the final state, $D_{\lambda_i \lambda_f}^J$ is an element of the Wigner rotation matrix [10], and the $*$ denotes complex conjugation. The resulting Ξ^- angular distribution integrated over ϕ is obtained for spin hypotheses $J_{\Xi(1530)} = 1/2, 3/2, \text{ and } 5/2$, respectively, as follows:

$$dN/d\cos\theta_{\Xi^-} \propto 1 + \beta \cos\theta_{\Xi^-}, \quad (2)$$

$$dN/d\cos\theta_{\Xi^-} \propto 1 + 3\cos^2\theta_{\Xi^-} + \beta \cos\theta_{\Xi^-} (5 - 9\cos^2\theta_{\Xi^-}), \quad (3)$$

$$dN/d\cos\theta_{\Xi^-} \propto 1 - 2\cos^2\theta_{\Xi^-} + 5\cos^4\theta_{\Xi^-} + \beta \cos\theta_{\Xi^-} (5 - 26\cos^2\theta_{\Xi^-} + 25\cos^4\theta_{\Xi^-}). \quad (4)$$

The coefficient of the asymmetric term,

$$\beta = \left[\frac{\rho_{1/2, 1/2} - \rho_{-1/2, -1/2}}{\rho_{1/2, 1/2} + \rho_{-1/2, -1/2}} \right] \left[\frac{|A_{1/2}^J|^2 - |A_{-1/2}^J|^2}{|A_{1/2}^J|^2 + |A_{-1/2}^J|^2} \right],$$

is zero as a consequence of parity conservation in the strong decay of $\Xi(1530)^0$ to $\Xi^- \pi^+$, which implies $|A_{1/2}^J| = |A_{-1/2}^J|$. It should be noted that Eqs. (2)–(4) do not depend on any assumption as to the parity of the $\Xi(1530)$.

The normalized angular distribution of the Ξ^- obtained from Eq. (1), and expressed explicitly in Eqs. (2)–(4) for $J = 1/2, 3/2, \text{ and } 5/2$, respectively, can be written in general as

$$\frac{dN}{d\cos\theta_{\Xi^-}} = N \left[\sum_{l=0}^{l_{\max}} \langle P_l \rangle P_l(\cos\theta_{\Xi^-}) \right], \quad (5)$$

where $l_{\max} = 2J - 1$, the value of each expansion coefficient $\langle P_l \rangle$ depends on J , and, if l is odd, $\langle P_l \rangle = 0$. The Legendre polynomials satisfy

$$\int_{-1}^1 d\cos\theta_{\Xi^-} P_i(\cos\theta_{\Xi^-}) P_j(\cos\theta_{\Xi^-}) = \delta_{ij}, \quad (6)$$

[i.e., $P_l(\cos\theta) = \sqrt{2\pi} Y_l^0(\cos\theta, \phi)$, where Y_l^0 is a spherical harmonic function], so that

$$\int_{-1}^1 \frac{dN}{d\cos\theta_{\Xi^-}} P_l(\cos\theta_{\Xi^-}) d\cos\theta_{\Xi^-} = N \langle P_l \rangle. \quad (7)$$

For a data distribution containing N events, the left-hand side of Eq. (7) is approximately equal to

$$\sum_{k=1}^N P_l(\cos\theta_{\Xi^-}^k),$$

since for large N , the sum over the observed events provides a good approximation to the integral; throughout this paper, this summation is termed “the $P_l(\cos\theta_{\Xi^-})$ moment” or simply “the P_l moment” of the data. Each assumption for J defines l_{\max} , so that $\langle P_l \rangle = 0$ for $l > l_{\max}$ and the $\langle P_l \rangle$ are calculable. For $J = 1/2, 3/2, 5/2$, $l_{\max} = 0, 2, 4$, with the corresponding $\langle P_{l_{\max}} \rangle$ values $1/\sqrt{2}$, $1/\sqrt{10}$, and $\sqrt{2}/7$, respectively. The relation

$$\sum_{k=1}^N \frac{P_{l_{\max}}(\cos\theta_{\Xi^-}^k)}{\langle P_{l_{\max}} \rangle} \approx N \quad (8)$$

implies that the number of $\Xi(1530)^0$ signal events in a given mass interval is well approximated if each event k is given weight

$$w_k = \frac{P_{l_{\max}}(\cos\theta_{\Xi^-}^k)}{\langle P_{l_{\max}} \rangle}, \quad (9)$$

after efficiency correction [11] and background subtraction.

Since the angular distribution shown in Fig. 2(b) is clearly not flat, $\Xi(1530)$ spin $1/2$ is ruled out. In order to test the $J = 3/2$ ($5/2$) hypothesis, each event is given a weight $w_k = \sqrt{10} P_2(\cos\theta_{\Xi^-}^k) [\frac{7}{\sqrt{2}} P_4(\cos\theta_{\Xi^-}^k)]$. Figure 3(a) shows the distribution of the $\sqrt{2} P_0(\cos\theta_{\Xi^-})$ moment which is just the efficiency-corrected distribution corresponding to Fig. 1(b) (the average efficiency is $\sim 27\%$). The $\sqrt{10} P_2(\cos\theta_{\Xi^-})$ and $7/\sqrt{2} P_4(\cos\theta_{\Xi^-})$ moments are shown in Figs. 3(b) and 3(c), respectively. Figure 3(b) indicates that spin $3/2$ is strongly favored, as essentially all of the $\Xi(1530)$ signal is retained. In contrast, the $7/\sqrt{2} P_4(\cos\theta_{\Xi^-})$ moment shown in Fig. 3(c) is consistent with zero in the $\Xi(1530)$ signal region, so that spin $5/2$ is clearly ruled out. The results for $l_{\max} \geq 6$ (not shown) are similar to those of Fig. 3(c). In order to quantify these results, the region $1.50 \leq m(\Xi^- \pi^+) \leq 1.65 \text{ GeV}/c^2$ is defined as the $\Xi(1530)$ signal region. The dashed curve of Fig. 3(a) corresponds to a fit to the region $m(\Xi^- \pi^+) \leq 1.66 \text{ GeV}/c^2$ with the signal region excluded; the fit function is a third order polynomial multiplied by phase space. This yields an estimated signal of $19\,159 \pm 581$ events. For

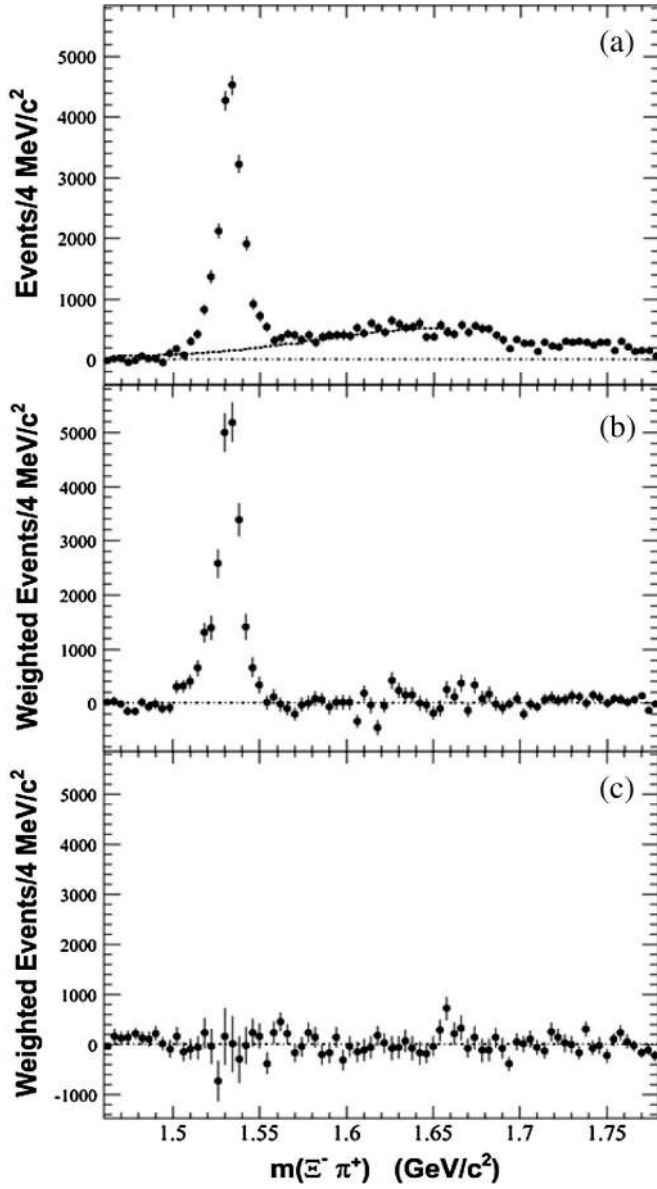


FIG. 3. The efficiency-corrected (a) $\sqrt{2}P_0(\cos\theta_{\Xi^-})$, (b) $\sqrt{10}P_2(\cos\theta_{\Xi^-})$, and (c) $7/\sqrt{2}P_4(\cos\theta_{\Xi^-})$ moments of the $\Xi^- \pi^+$ system invariant mass distribution for the Λ_c^+ signal region. In (a) the dashed curve represents the estimated background contribution in the $\Xi(1530)$ region, obtained as described in the text.

Figs. 3(b) and 3(c), the moment sums for the signal region are $23\,355 \pm 894$ and 78 ± 1410 , respectively. Clearly, $J = 3/2$ is the only viable $\Xi(1530)$ spin value. It follows that, based on the results of Refs. [2,3] (i.e., $J^P = 3/2^+$ or $J^P = 5/2^-$), the present analysis, which shows that $J = 3/2$, also establishes positive parity, and that the $\Xi^- \pi^+$ system which results from the decay is in a P -wave orbital angular momentum state. Here, and in Refs. [2,3], it is assumed that the Ξ^- has positive parity [1].

The distributions for the sideband regions which correspond to those of Fig. 3 for the signal region are shown in

Fig. 4. Although Fig. 4(a) shows a small $\Xi(1530)^0$ signal, Fig. 4(b) demonstrates that the angular distribution is not as expected for Λ_c^+ decay. This lack of coherence with the Λ_c^+ signal justifies the removal of background in the signal region by means of the sideband subtraction procedure described previously in this section. Figure 4(c) is very similar to Fig. 3(c) in that neither shows evidence of any significant structure.

The correlation between the Λ_c^+ signal and the angular distribution in the $\Xi(1530)^0$ region is demonstrated very clearly in Fig. 5. Each event in Fig. 1(a) is given weight $\sqrt{10}P_2(\cos\theta_{\Xi^-})$, and each data point in Fig. 5 represents the sum of weights in the relevant mass interval. The sideband regions, and indeed all of the background contributions, sum to ~ 0 , and only the Λ_c^+ signal survives.

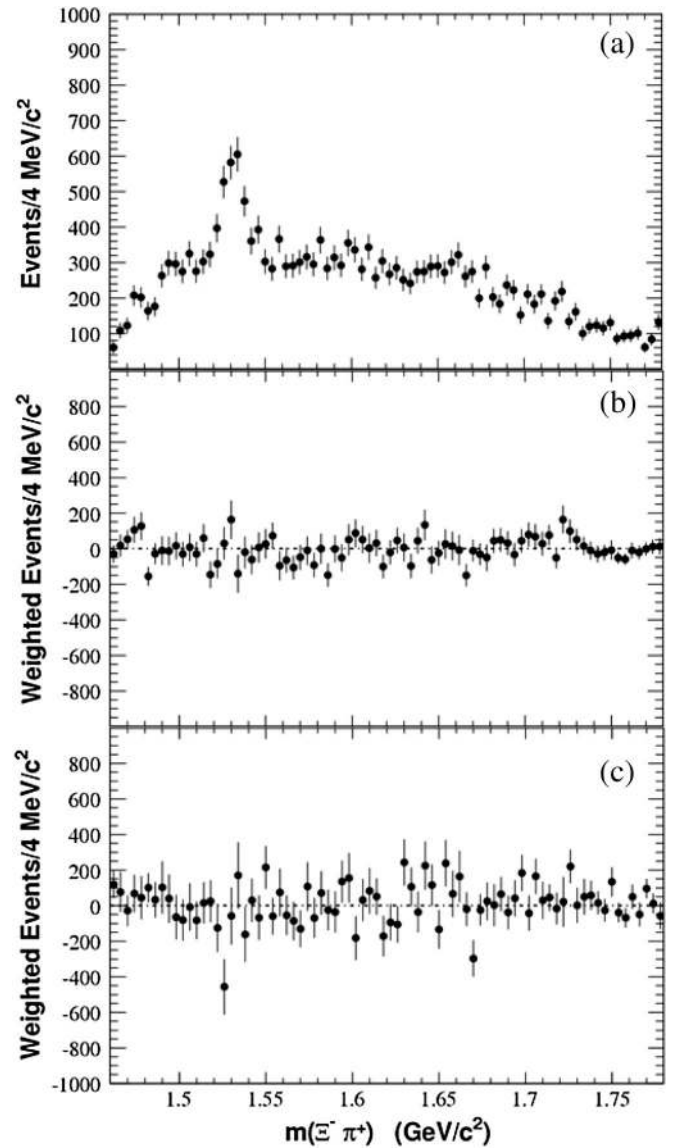


FIG. 4. The efficiency-corrected distributions corresponding to those of Fig. 3, but for the Λ_c^+ sideband regions indicated in Fig. 1(a).

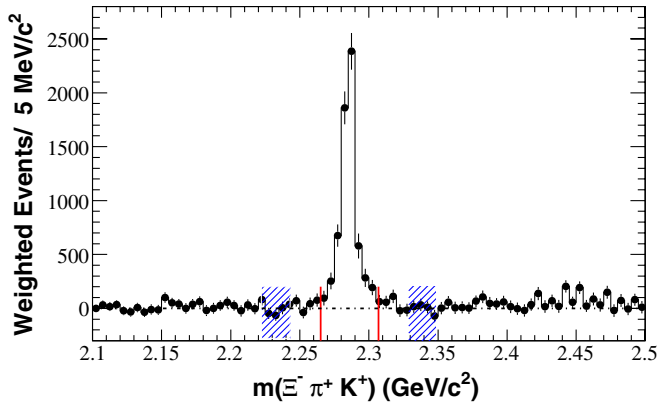


FIG. 5 (color online). The uncorrected $\Xi^- \pi^+ K^+$ invariant mass distribution corresponding to Fig. 1(a) after weighting each event by $\sqrt{10}P_2(\cos\theta_{\Xi^-})$. The solid lines and shaded areas delimit the signal region and mass-sideband regions, respectively.

IV. THE $\Xi(1530)$ MASS REGION

Although Fig. 3 clearly establishes spin 3/2 for the $\Xi(1530)$, the analysis of the $\Xi^- \pi^+$ system described in the remainder of this paper indicates that a detailed understanding of the data is much less straightforward than Fig. 3 might indicate. If the momentum of the Ξ^- in the $\Xi^- \pi^+$ r.f. is denoted by q , a Breit-Wigner (BW) amplitude corresponding to orbital angular momentum L should be proportional to the centrifugal barrier factor q^L [12]. The line shape for a $\Xi^- \pi^+$ P -wave BW amplitude should then be skewed toward high-mass values. However, the distribution of Fig. 3(b), which should represent the square of a P -wave amplitude, appears to be skewed toward low-mass values, in contradiction to this expectation. Furthermore, if the distribution in Fig. 3(a) is considered to represent a sum of squares of $\Xi^- \pi^+$ amplitudes, for which that in Fig. 3(b) represents the $J = 3/2$ contribution, their difference would be expected to behave like the background distribution in Fig. 3(a) in the $\Xi(1530)^0$ region. However, the $\Xi(1530)$ signal in Fig. 3(b) contains ~ 4000 events more than that in Fig. 3(a), as indicated above, so that when the former is subtracted from the latter, the residual distribution exhibits a strong dip in the $\Xi(1530)$ region, and even reaches negative values. This behavior is clearly at odds with a simple interpretation of these distributions.

Moreover, the $\cos\theta_{\Xi^-}$ distribution in the $\Xi(1530)^0$ signal region indicates that a description in terms of a single $\Xi^- \pi^+$ amplitude corresponding to a resonant structure is an over-simplification. The Λ_c^+ mass-sideband-subtracted $\cos\theta_{\Xi^-}$ distribution for the $\Xi(1530)^0$ signal region (Fig. 6) exhibits a predominantly quadratic behavior, which indicates clearly that the spin of the $\Xi(1530)$ is not 1/2. A function $\propto (1 + 3\cos^2\theta)$ [solid curve of Fig. 6(b), the parametrization of Eq. (3)] which corresponds to $J = 3/2$ for the $\Xi(1530)^0$ fits the data best, although there are clear deviations from the curve, and the fit confidence level

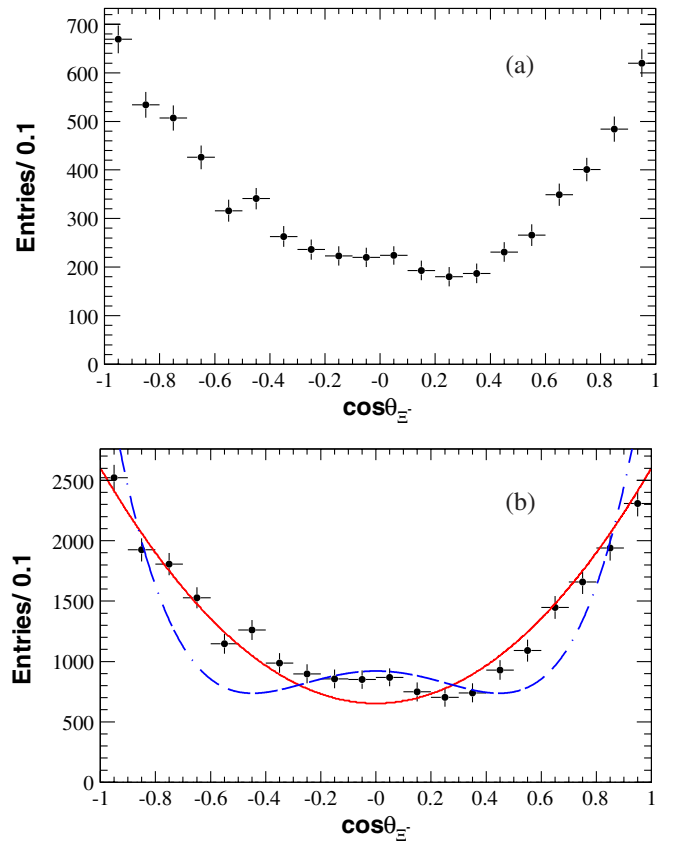


FIG. 6 (color online). The $\cos\theta_{\Xi^-}$ distribution for $\Lambda_c^+ \rightarrow \Xi^- \pi^+ K^+$ data in the $\Xi(1530)^0 \rightarrow \Xi^- \pi^+$ signal region (a) before and (b) after efficiency correction. The solid (dashed) curve corresponds to the parametrization of the $\Xi(1530)$ angular distribution for the assumption of *pure* spin 3/2 (5/2).

(c.l.) is only 0.0003. The fit with the parametrization which corresponds to $J = 5/2$ [dashed curve, Eq. (4)] is extremely poor, with c.l. 6×10^{-44} , as would be expected from the projection of Fig. 3(c). In addition, the distribution of Fig. 6(b) exhibits signs of forward-backward asymmetry.

The above symptoms indicate that a more complicated description is required if a quantitative understanding of the $\Xi^- \pi^+$ system is to be achieved.

Strong interactions in the $\Xi^- \pi^+$ system may give rise to interference between the resonant P -wave $\Xi(1530)$ amplitude and other $\Xi^- \pi^+$ amplitudes. Evidence for interference is seen in the behavior of the $P_1(\cos\theta_{\Xi^-})$ moment of the $\Xi^- \pi^+$ system as a function of invariant mass. The distribution shown in Fig. 7 is consistent with the interference pattern resulting from the rapid oscillation due to $\Xi(1530)$ P -wave BW phase motion in the presence of an amplitude with small, slowly varying, relative phase; the projection would then approximate the real part of the BW amplitude, as observed.

The oscillatory pattern seen in Fig. 7 is not observed for the high- and low- Λ_c^+ -mass-sideband regions, which confirms that the pattern is indeed due to $\Xi(1530)$ phase

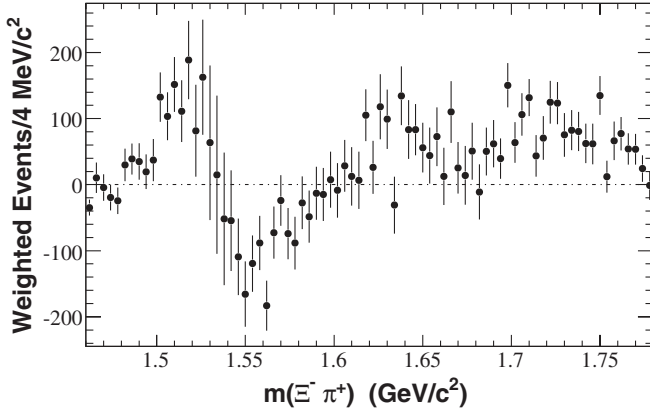


FIG. 7. The efficiency-corrected $P_1(\cos\theta_{\Xi^-})$ moment of the $\Xi^- \pi^+$ system invariant mass distribution corresponding to the Λ_c^+ signal region. The distributions for the sideband regions are consistent with zero, and so are not subtracted.

motion in events produced from signal Λ_c^+ candidates, and is not simply an artifact of combinatorial background. As mentioned above, the $P_1(\cos\theta_{\Xi^-})$ moment for $m(\Xi^- \pi^+) < 1.58 \text{ GeV}/c^2$ behaves very much like the real part of the $\Xi(1530)$ BW amplitude, which suggests that the phase of the amplitude yielding the interference effect is close to zero. The proximity of $\Xi^- \pi^+$ threshold and the fact that the interference is seen in the $P_1(\cos\theta_{\Xi^-})$ moment suggest that the effect is due primarily to the presence of an S -wave $\Xi^- \pi^+$ amplitude.

If it is assumed that only total spin $J = 1/2$ and $3/2$ amplitudes contribute, and if the description is restricted to S , P , and D waves, the following angular distribution for the Ξ^- produced in $\Xi^- \pi^+$ decay is obtained:

$$\begin{aligned} \frac{dN}{d\cos\theta_{\Xi^-}} = & \left[\frac{1}{2} |S^{1/2}|^2 + |P^{3/2}|^2 \left(\frac{1 + 3\cos^2\theta_{\Xi^-}}{4} \right) \right. \\ & \left. + \sqrt{2} \text{Re}(S^{1/2}P^{3/2*}) \cos\theta_{\Xi^-} \right] \\ & + \left[\frac{1}{2} |P^{1/2}|^2 + |D^{3/2}|^2 \left(\frac{1 + 3\cos^2\theta_{\Xi^-}}{4} \right) \right. \\ & \left. + \sqrt{2} \text{Re}(P^{1/2}D^{3/2*}) \cos\theta_{\Xi^-} \right] \end{aligned} \quad (10)$$

where the amplitude notation is L^J .

The angular structure associated with the $J = L + 1/2$ terms [Eq. (10), first set of brackets] is identical to that associated with the $J = L - 1/2$ terms [Eq. (10), second set of brackets]; i.e., there is a Minami ambiguity [13]. It follows that there are more unknown quantities than measurables, so that a complete set of amplitudes cannot be extracted from the data. However, since the $\Xi(1530)$ is a $P^{3/2}$ resonance, it is reasonable to attribute the $P_1(\cos\theta_{\Xi^-})$ moment behavior of Fig. 7 to the $S^{1/2}$ - $P^{3/2}$ interference term of Eq. (10); in addition, D -wave amplitudes would not be expected to be significant for $\Xi^- \pi^+$ mass values

close to threshold, so that a simple model which incorporates only $S^{1/2}$ and $P^{3/2}$ amplitudes might describe the data. This would imply that the intensity distribution of Fig. 3(b) corresponds to $|P^{3/2}|^2$ only. However, as discussed above, the difference in the distributions of Figs. 3(a) and 3(b) dips strongly in the $\Xi(1530)$ region, even reaching negative values, and so cannot be described by $|S^{1/2}|^2$. This indicates that the data in the $\Xi(1530)$ mass region require a more complicated explanation.

V. THE $\Xi^- \pi^+$ SYSTEM AT HIGHER MASS

The inclusion of a $D^{3/2}$ contribution [Eq. (10)] does not solve the problem of the $\Xi(1530)$ mass region described at the end of Sec. IV, since Fig. 3(b) then corresponds to $|P^{3/2}|^2 + |D^{3/2}|^2$ and Fig. 3(a) to $|S^{1/2}|^2 + |P^{3/2}|^2 + |D^{3/2}|^2$. If the model is extended to include a $D^{5/2}$ amplitude, the Legendre polynomial moments, P_0 - P_4 , are expressed in terms of the amplitudes as follows:

$$P_0 = \frac{1}{\sqrt{2}} [|S^{1/2}|^2 + |P^{1/2}|^2 + |P^{3/2}|^2 + |D^{3/2}|^2 + |D^{5/2}|^2], \quad (11)$$

$$P_1 = \frac{2}{\sqrt{3}} [\text{Re}(S^{1/2}P^{3/2*}) + \text{Re}(P^{1/2}D^{3/2*})] + \frac{6}{5} \text{Re}(P^{3/2}D^{5/2*}), \quad (12)$$

$$P_2 = \frac{1}{\sqrt{10}} \left[|P^{3/2}|^2 + |D^{3/2}|^2 + \frac{8}{7} |D^{5/2}|^2 + \sqrt{20} \text{Re}(S^{1/2}D^{5/2*}) \right], \quad (13)$$

$$P_3 = \frac{4}{5} \sqrt{\frac{3}{7}} \text{Re}(P^{3/2}D^{5/2*}), \quad (14)$$

$$P_4 = \frac{\sqrt{2}}{7} |D^{5/2}|^2. \quad (15)$$

These five equations involve nine unknown quantities (five amplitude magnitudes and four relative phase angles), and so cannot be solved. Additional input from polarization moments is required. Such an analysis is beyond the scope of the present paper. If we assume that the $P^{1/2}$ and $D^{3/2}$ amplitudes can be ignored, Eqs. (11), (12), (14), and (15) can be solved, in principle. However, as is discussed below, even such a simplified model encounters difficulties in the $\Xi(1530)$ region.

In the context of this model, the absence of any significant P_4 moment in Fig. 3(c) indicates via Eq. (15) that $|D^{5/2}|$ must be small. However, since $P^{3/2}$ is large, $P^{3/2}$ - $D^{5/2}$ interference might be seen in the mass dependence of the P_3 moment [Eq. (14)]. This is shown in Fig. 8, where

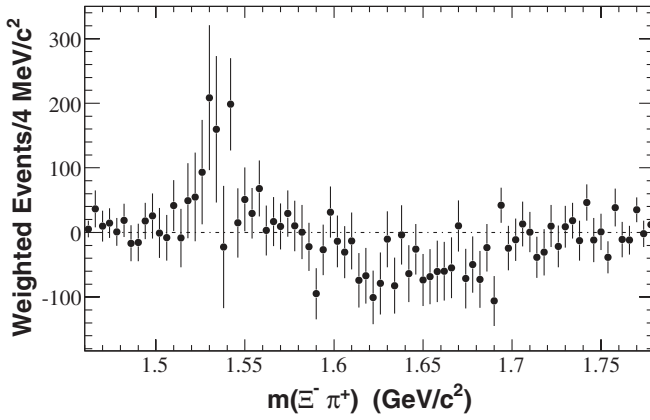


FIG. 8. The efficiency-corrected $P_3(\cos\theta_{\Xi^-})$ moment of the $\Xi^- \pi^+$ invariant mass distribution for the Λ_c^+ signal region. The distributions for the sideband regions are consistent with zero, and so are not subtracted.

small, but significant, deviations from zero are in fact observed. Since there is a $P^{3/2} - D^{5/2}$ interference contribution to Eq. (12), an improved measure of the mass dependence of $S^{1/2} - P^{3/2}$ interference is obtained by subtracting $(\sqrt{21}/2)P_3$ from P_1 . The $P_1 - (\sqrt{21}/2)P_3$ distribution is shown in Fig. 9, and the dip in the mass region 1.63–1.70 GeV/c^2 of Fig. 7 has been removed by this procedure. Before the $\Xi(1530)$ region is examined in more detail, the behavior of $P_1 - (\sqrt{21}/2)P_3$ is considered in the mass region above $\sim 1.6 \text{ GeV}/c^2$.

It is interesting to consider this in comparison to the distribution of Fig. 3(a) with the $\Xi(1530)$ region suppressed (Fig. 10), which shows a significant decrease in intensity at $\sim 1.7 \text{ GeV}/c^2$. As mentioned previously, the behavior of the P_1 moment in the $\Xi(1530)$ region indicates a small $S^{1/2}$ amplitude with phase ~ 0 deg relative to the $P^{3/2}$ amplitude in order that P_1 closely resemble the real

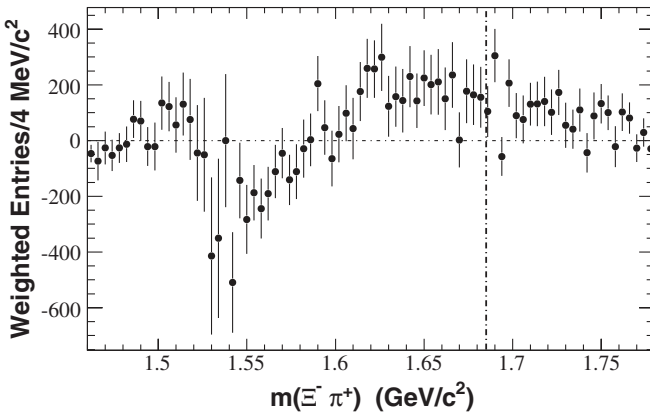


FIG. 9. The efficiency-corrected $P_1 - (\sqrt{21}/2)P_3$ moment of the $\Xi^- \pi^+$ system invariant mass distribution, corresponding to the Λ_c^+ signal region. The dot-dashed line indicates the $\Xi(1690)^0$ mass value [1]. The distributions for the sideband regions are consistent with zero, and so are not subtracted.

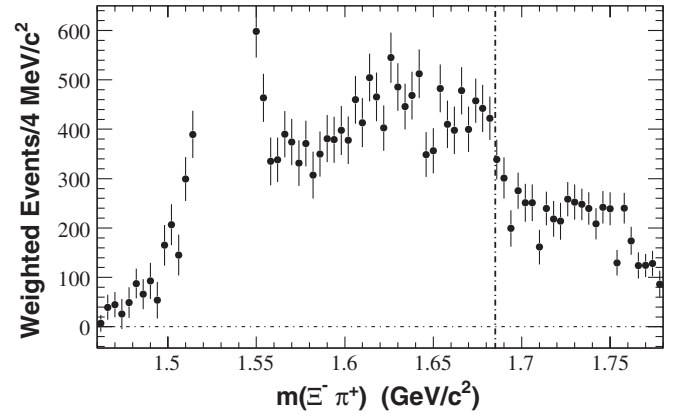


FIG. 10. The efficiency-corrected Λ_c^+ mass-sideband-subtracted $P_0(\cos\theta_{\Xi^-})$ moment of the $\Xi^- \pi^+$ system invariant mass distribution for the Λ_c^+ signal region [the distribution of Fig. 3(a) with the $\Xi(1530)$ region suppressed]. The vertical dashed line indicates the $\Xi(1690)^0$ mass value [1].

part of the $\Xi(1530)$ BW amplitude. If the $S^{1/2}$ amplitude did not change significantly at higher mass values, the BW amplitude would cause P_1 to approach zero from below with increasing mass. Instead, P_1 passes through zero at $\sim 1.6 \text{ GeV}/c^2$ and remains positive thereafter (Fig. 9). Since P_1 represents the projection of the $S^{1/2}$ amplitude onto the $P^{3/2}$ amplitude, this means that the $S^{1/2}$ phase is increasing significantly, is only 90 deg behind the $P^{3/2}$ phase at $\sim 1.6 \text{ GeV}/c^2$ where P_1 is ~ 0 , and continues to increase at higher mass. The dip in the mass distribution of Fig. 10 is in the vicinity of the $\Xi(1690)$, which is known to have a small coupling to $\Xi^- \pi^+$ [14]. This dip could occur as the result of the coherent addition of a small, resonant $\Xi(1690)$ amplitude to the slowly increasing $S^{1/2}$ amplitude, as shown schematically by the cartoon of Fig. 11. Here the large circle represents a slowly varying nonresonant $S^{1/2}$ amplitude for which the phase reaches 90 deg at mass $\sim 1.6 \text{ GeV}/c^2$, relative to a $P^{3/2}$ amplitude; the latter should be approximately aligned with the negative real axis at this mass value. As the phase increases beyond 90 deg, the $S^{1/2}$ projection on the $P^{3/2}$ amplitude [i.e., P_1] will increase as seen in Fig. 9. The small circle represents the subsequent coherent addition of a small resonant $\Xi(1690)$ amplitude. The resultant amplitude will then yield a dip in overall intensity in the $\Xi(1690)$ region with very little effect on the phase, and hence on P_1 (cf. Fig. 9). The inference which can be drawn is that the $\Xi(1690)$ decays strongly to the $\Xi^- \pi^+$ system in an S -wave orbital state, and hence that it has spin-parity $1/2^-$. As such, this represents the first experimental information on the spin-parity of the $\Xi(1690)$. Spin 1/2 is favored also by an analysis of the Dalitz plot corresponding to the decay process $\Lambda_c^+ \rightarrow \Lambda \bar{K}^0 K^+$ [15].

The behavior of the $S^{1/2}$ amplitude described above is remarkably similar to that obtained for the $I = 1/2$ S -wave

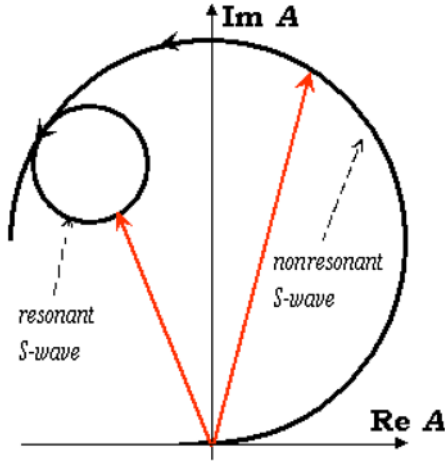


FIG. 11 (color online). A cartoon of an Argand diagram which illustrates a possible cause for the dip in the $\Xi^- \pi^+$ invariant mass distribution due to the presence of the $\Xi(1690)^0 \rightarrow \Xi^- \pi^+$.

$K^- \pi^+$ scattering amplitude in the LASS experiment [16]. There, the slow, monotonic increase in the S -wave amplitude at low mass is described by an effective range parametrization. The phase reaches ~ 90 deg before the coherent addition of a resonant $K_0^*(1430)$ contribution takes effect, and the resultant amplitude decreases quickly almost to zero. The main difference in the $K^- \pi^+$ case is that the resultant amplitude remains elastic (within error) up to $K \eta'$ threshold, so that the decrease in S -wave intensity is quite substantial. Since the $\Xi(1690)$ decays significantly via modes other than $\Xi^- \pi^+$, a similar mechanism would be expected to yield less dramatic results, as is in fact observed in Fig. 10. This similarity between $K \pi$ and $\Xi \pi$ scattering amplitudes may be an example of the proposed effective supersymmetry between mesons and baryons involving the replacement of a light antiquark in the meson by a light diquark to form the related baryon [17]. For $I = 1/2$, the amplitudes describing $K^- \pi^+$ scattering are the same as for $K^+ \pi^-$, and similarly those describing $\Xi^- \pi^+$ scattering are proportional to those for $\Xi^0 \pi^-$ scattering; $K^+ \pi^-$ scattering is then converted to $\Xi^0 \pi^-$ scattering by replacing the \bar{s} quark in the K^+ with an (ss) diquark to obtain the Ξ^0 . In Ref. [17], the effective symmetry is demonstrated by relating various baryon-baryon and meson-meson mass differences with impressive precision. It seems reasonable to conjecture that this symmetry might also be manifest in the dynamics of appropriately related meson-meson and baryon-meson scattering processes.

VI. THE $\Xi(1530)^0$ LINE SHAPE

In the $\Xi(1530)$ region, $S^{1/2} - D^{5/2}$ interference does in fact contribute to the P_2 moment distribution in Fig. 3(b) [cf. Eq. (13)], but not to the distribution in Fig. 3(a) [cf. Eq. (11)], so that the $\Xi(1530)$ signal in Fig. 3(b) might be larger than that in Fig. 3(a). In addition, this contribution

might distort the line shape in Fig. 3(b), but should not affect that in Fig. 3(a), which is obtained by integration over $\cos\theta_{\Xi^-}$. In order to test this conjecture, fits to the distributions in Figs. 3(a) and 3(b) are performed in which the $\Xi(1530)$ line shape is described by

$$\frac{dN}{dm} = C \frac{(p^{2L}/D_L(p, R))(q^{2l}/D_l(q, R))}{(m_0^2 - m^2)^2 + m_0^2 \Gamma_{\text{tot}}(m)^2} p \cdot q, \quad (16)$$

where C is a constant, p is the momentum of the K^+ in the Λ_c^+ r.f., and q is the momentum of the Ξ^- in the $\Xi^- \pi^+$ r.f.; L is the orbital angular momentum in the Λ_c^+ decay ($L = 1$ is chosen), and l that in the $\Xi(1530)$ decay (for which $l = 1$); D_L, D_l are Blatt-Weisskopf barrier factors [12] with radius parameter R , and, for example, $D_1(q, R) = 1 + (qR)^2$; and $R = 3 \text{ GeV}^{-1}$ ($\sim 0.6 \text{ f}$) is chosen [16]. The $\Xi(1530)$ mass is m_0 , and $\Gamma_{\text{tot}}(m)$ its mass-dependent total width, which consists of the sum of partial widths to $\Xi^0 \pi^0$ and $\Xi^- \pi^+$. If the particle mass differences between these modes are ignored, the mass-dependent total width is then

$$\Gamma_{\text{tot}}(m) = \Gamma_0 \frac{q}{q_0} \frac{m_0}{m} \frac{q^2}{D_1(q, R)} \frac{D_1(q_0, R)}{q_0^2}, \quad (17)$$

where Γ_0 is the width of the $\Xi(1530)$, and $q_0 = q(m_0)$. For the fits to the data of Fig. 3(a), an incoherent background function of the form

$$b = (p \cdot q) \sum_{i=0}^3 c_i m^i \quad (18)$$

is included also.

In each fit, the fit function is convolved with a mass resolution function consisting of two Gaussian distributions with a common center and fixed fractional contributions, but with r.m.s. deviation values which depend on $\Xi^- \pi^+$ invariant mass. For the resolution function, the resulting half-width-at-half-maximum increases from $\sim 0.5 \text{ MeV}/c^2$ just above threshold to $\sim 1.5 \text{ MeV}/c^2$ at the $\Xi(1530)$, reaching $\sim 2.5 \text{ MeV}/c^2$ at $\sim 1.6 \text{ GeV}/c^2$, so that the resolution in the signal region is excellent. The degradation of the mass resolution with increasing $\Xi^- \pi^+$ mass should, if anything, cause the observed $\Xi(1530)^0$ line shape to be slightly skewed toward high mass; it follows that this cannot be the source of the skewing of the line shapes of Figs. 3(a) and 3(b) toward low mass. The convolution procedure takes quantitative account of the resolution behavior, but, since the resolution is excellent, this has little impact on the description of the data. The fit results with $\Xi(1530)^0$ mass and width fixed at their PDG values [1] are shown in Fig. 12. In Figs. 12(a) and 12(c), the dots represent the data of Figs. 3(a) and 3(b), respectively, while the histograms represent the mass-resolution-smearred fit functions integrated over the corresponding mass intervals. The fit residuals (data - histogram) are shown in Figs. 12(b) and 12(d), respec-

tively. These show similar, very large, systematic deviations from zero, and the fits have correspondingly poor c.l. values (6×10^{-16} and ~ 0 , respectively). With the mass and width parameters free in the fits, the c.l. values are still poor, and the values obtained differ significantly from the PDG values [e.g., $m_0 = 1534.4 \pm 0.1 \text{ MeV}/c^2$ and $\Gamma_0 = 13.2 \pm 0.5 \text{ MeV}$ for Fig. 12(a)]. If the Blatt-Weisskopf radius parameter is allowed to be free, an acceptable fit to the mass distribution is not obtained (c.l. $\sim 10^{-3}$), the residuals still show systematic deviations from zero, and the mass and width values obtained still differ significantly from their PDG values. Similarly, the fit to the P_2 moment mass dependence with mass, width, and radius parameters free remains poor (c.l. $\sim 10^{-7}$); in addition, the radius parameter increases to $\sim 100 \text{ GeV}^{-1}$ (which is equivalent to the use of an S -wave Breit-Wigner amplitude) in an attempt to reproduce the observed lack of skewing toward high mass expected for a P -wave decay. Since the P -wave nature of the decay has been established, this is certainly an unacceptable result.

As a check of the signal parametrization of Eq. (16), this function (with $R = 3 \text{ GeV}^{-1}$) has been used in fits to the published $\Xi^- \pi^+$ mass distributions from four of the experiments [18–21] used to obtain the PDG mass and width values [1]. These are hydrogen bubble chamber experiments, and each mass distribution is obtained as the projection of the Dalitz plot for the reaction $K^- p \rightarrow \Xi^- \pi^+ K^0$ (Ref. [19] uses some additional contributions). The analysis samples are small (125, 350, 324, and 1313 events, respectively), and the details of the fit functions used in Refs. [18–21] are not made clear. It is found that the nonresonant background contributions are well described using only the $(p \cdot q)$ phase space factor of Eq. (18), and Eq. (16), convolved with a Gaussian of r.m.s. deviation specified for each experiment, is used to represent the $\Xi(1530)$ signal. Good c.l. values are obtained, and the resulting weighted average mass ($1532.2 \pm 0.2 \text{ MeV}/c^2$) and width ($9.9 \pm 0.5 \text{ MeV}$) values agree well with those from the PDG [1]. This indicates that the choice of signal and background functions is not the reason for the poor-quality fits to the data of Fig. 12. Furthermore, since no significant improvement in fit quality is observed in going from the P_2 fit to the P_0 fit, it follows that the difficulty in fitting the former cannot be attributed to the presence of an $S^{1/2} - D^{5/2}$ interference contribution, since this would not be present for the latter.

This striking failure to describe the most obvious feature of the $\Xi^- \pi^+ K^+$ Dalitz plot leads to the conclusion that a satisfactory description of the observed $[m(\Xi^- \pi^+), \cos\theta_{\Xi^-}]$ distribution cannot be obtained in terms of amplitudes pertaining solely to the $\Xi^- \pi^+$ system. The difficulties probably result from overlap and interference effects involving amplitudes associated with the $K^+ \pi^+$ and/or the $\Xi^- K^+$ systems (if the possibility of direct three-body decay is ignored). The $K^+ \pi^+$ system has $I = 3/2$, and

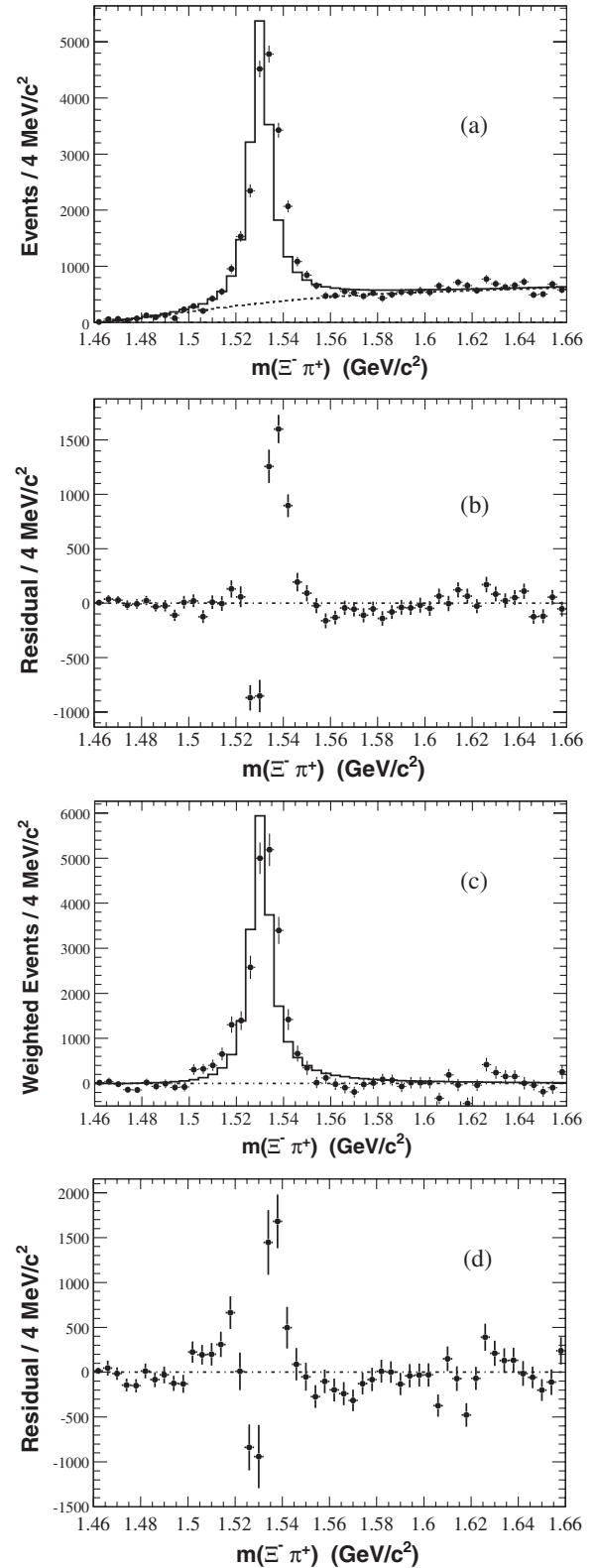


FIG. 12. The efficiency-corrected Λ_c^+ -mass-sideband-subtracted (a) $\sqrt{2}P_0(\cos\theta_{\Xi^-})$ and (c) $\sqrt{10}P_2(\cos\theta_{\Xi^-})$ moment distributions for the $\Xi^- \pi^+$ system, for the Λ_c^+ signal region (solid dots). The fits represented by the histograms are described in the text. In (b) [(d)] the difference between the data points and the histogram in (a) [(c)] is shown.

has been observed to have only an S -wave amplitude, which varies slowly with mass in the relevant region ($\leq 1 \text{ GeV}/c^2$). It seems unlikely that such an amplitude could lead to significant distortion of the mass and $\cos\theta_{\Xi^-}$ dependences of the $\Xi^- \pi^+$ system, but the relevant quantitative analysis has not yet been attempted. In contrast, the $\Xi^- K^+$ system could have contributions from high-mass Λ or Σ^0 resonant structures in the region of overlap with the $\Xi(1530)$ [$> 2 \text{ GeV}/c^2$, cf. Fig. 2(a)]. Very little is known about such states or their couplings to $\Xi^- K^+$ [1], and there is no clear evidence for their presence in the Dalitz plots of Fig. 2. Indeed, the only “evidence” for such contributions is the failure of the description of the $\Xi(1530)$ region solely in terms of $\Xi^- \pi^+$ amplitudes in the present analysis. This seeming impasse might benefit from analyses of related Λ_c^+ decay processes, such as $\Lambda_c^+ \rightarrow (\Lambda \eta) \pi^+$ or $\Lambda_c^+ \rightarrow (\Lambda \pi^0) \pi^+$, although these may suffer from their own particular complications related to other quasi-two-body modes.

VII. CONCLUSION

In conclusion, the analysis of the Legendre polynomial moments of the $\Xi^- \pi^+$ system which result from data on the decay $\Lambda_c^+ \rightarrow \Xi^- \pi^+ K^+$ has established quite clearly, on the basis of Figs. 3(b) and 3(c), that the $\Xi(1530)$ hyperon resonance has spin $3/2$. In conjunction with previous analyses [2,3], this also definitively establishes positive parity, and hence that the $\Xi(1530)$ is a $P^{3/2}$ resonance. However, comparison of the $P_2(\cos\theta_{\Xi^-})$ moment to the $\Xi^- \pi^+$ mass distribution and fits to the angular decay distribution in the $\Xi(1530)$ region indicate that it is necessary to include other $\Xi^- \pi^+$ amplitudes in order to obtain a complete description of the data. In particular, the observation of a $P_1(\cos\theta_{\Xi^-})$ moment exhibiting oscillatory behavior in the $\Xi(1530)^0$ region indicates the need for an $S^{1/2}$ amplitude, while providing first evidence for the expected rapid BW phase motion of the $P^{3/2}$ $\Xi(1530)^0$ amplitude. However, a simple model incorporating only these amplitudes and a $D^{5/2}$ amplitude is ruled out because

of the failure to describe the $\Xi(1530)^0$ line shape. The presence of the $S^{1/2}$ amplitude at high mass and the behavior of the mass distribution at $\sim 1.7 \text{ GeV}/c^2$ suggest that a resonant $\Xi(1690)^0$ amplitude may be adding coherently to this amplitude, thus leading to the inference of spin-parity $1/2^-$ for the $\Xi(1690)$. It appears that a quantitative description of the $\Xi(1530)$ line shape, and indeed of the entire Dalitz plot, must incorporate these features together with amplitude contributions associated with the $K^+ \pi^+$ and/or the $\Xi^- K^+$ systems. An analysis of this complexity will be performed when the full *BABAR* data sample (integrated luminosity approximately 500 fb^{-1}) is available.

ACKNOWLEDGMENTS

We are grateful for the extraordinary contributions of our PEP-II colleagues in achieving the excellent luminosity and machine conditions that have made this work possible. The success of this project also relies critically on the expertise and dedication of the computing organizations that support *BABAR*. The collaborating institutions wish to thank SLAC for its support and the kind hospitality extended to them. This work is supported by the U.S. Department of Energy and National Science Foundation, the Natural Sciences and Engineering Research Council (Canada), the Commissariat à l’Energie Atomique and Institut National de Physique Nucléaire et de Physique des Particules (France), the Bundesministerium für Bildung und Forschung and Deutsche Forschungsgemeinschaft (Germany), the Istituto Nazionale di Fisica Nucleare (Italy), the Foundation for Fundamental Research on Matter (The Netherlands), the Research Council of Norway, the Ministry of Education and Science of the Russian Federation, Ministerio de Educación y Ciencia (Spain), and the Science and Technology Facilities Council (United Kingdom). Individuals have received support from the Marie-Curie IEF program (European Union) and the A. P. Sloan Foundation.

-
- [1] W.-M. Yao *et al.* (PDG2006), J. Phys. G **33**, 1 (2006).
 - [2] P. Schlein *et al.*, Phys. Rev. Lett. **11**, 167 (1963).
 - [3] J. Button-Shafer *et al.*, Phys. Rev. **142**, 883 (1966).
 - [4] B. Aubert *et al.* (*BABAR* Collaboration), Phys. Rev. Lett. **97**, 112001 (2006).
 - [5] The use of charge conjugate reactions is implied throughout this paper.
 - [6] B. Aubert *et al.*, Nucl. Instrum. Methods Phys. Res., Sect. A **479**, 1 (2002).
 - [7] The signal and low- and high-mass-sideband regions correspond to [2.265, 2.307], and [2.223, 2.244], [2.328, 2.349] GeV/c^2 , respectively.
 - [8] M. Jacob and G. C. Wick, Ann. Phys. (Leipzig) **7**, 404 (1959).
 - [9] S. U. Chung, CERN Yellow Report No. CERN 71-8, 1971.
 - [10] E. Wigner, *Gruppentheories* (Freidrich Vieweg und Sohn,

- Braunschweig, 1931); *Group Theory* (Academic Press, New York, 1959).
- [11] Each selected event is weighted by the inverse value of its calculated efficiency, which is parametrized as a function of $\cos(\theta_{\Xi^-})$ and $m(\Xi^- \pi^+)$ using $\Lambda_c^+ \rightarrow \Xi^- \pi^+ K^+$ signal Monte Carlo events.
- [12] J.M. Blatt and V.F. Weisskopf, *Theoretical Nuclear Physics* (John Wiley and Sons, New York, 1952).
- [13] S. Minami, *Prog. Theor. Phys.* **11**, 213 (1954).
- [14] M.I. Adamovich *et al.*, *Eur. Phys. J. C* **5**, 621 (1998).
- [15] Veronique Ziegler, Ph.D. thesis [SLAC Report No. SLAC-R-868, 2007].
- [16] D. Aston *et al.*, *Nucl. Phys.* **B296**, 493 (1988).
- [17] M. Karliner and H. Lipkin, *Phys. Lett. B* **660**, 539 (2008).
- [18] G.W. London *et al.*, *Phys. Rev.* **143**, 1034 (1966).
- [19] L. Kirsch *et al.*, *Nucl. Phys.* **B40**, 349 (1972).
- [20] S. Borenstein *et al.*, *Phys. Rev. D* **5**, 1559 (1972).
- [21] C. Baltay *et al.*, *Phys. Lett.* **42B**, 129 (1972).